J. Fluid Mech. (2007), *vol.* 573, *pp.* 149–169.
doi:10.1017/S0022112006003739 Printed in the United Kingdom

Hydrodynamic interaction between two identical capsules in simple shear flow

ETIENNE LAC, ARNAUD MOREL AND DOMINIQUE BARTHÈS-BIESEL

UMR CNRS 6600, Biomécanique et Génie Biomédical, Université de Technologie de Compiègne, France

(Received 7 December 2005 and in revised form 1 August 2006)

We present a numerical model of the hydrodynamic interactions between two capsules freely suspended in a simple shear flow. The capsules are identical and each consists of a liquid droplet enclosed by a thin hyperelastic membrane, devoid of bending resistance and obeying a neo-Hookean constitutive law. The two capsules are slightly prestressed with a given inflation ratio in order to avoid the small deformation instability due to compression observed for a single capsule in simple shear flow. The viscosity ratio between the interior and exterior fluids of the capsule is taken to be unity and creeping flow conditions are assumed to prevail. The boundary-element method is used with bi-cubic B-splines as basis functions on a structured mesh in order to discretize the capsule surface. A new method using two grids with initially orthogonal pole axes is developed to eliminate polar singularities in the load calculation and to allow for long computation times. Two capsules suspended in simple shear flow usually have different velocities and thus eventually pass each other. We study this crossing process as a function of flow strength and initial particle separation. We find that hydrodynamic interactions during crossing lead to large shape alterations, elevated elastic tensions in the membrane and result in an irreversible trajectory shift of the capsules. Furthermore, a tendency towards buckling is observed, particularly during the separation phase where large pressure differences occur. Our results are in qualitative agreement with those obtained for a pair of interacting liquid droplets but show the specific role played by the membrane of capsules.

1. Introduction

Artificial capsules consisting of a liquid droplet enclosed by a thin elastic membrane are widely used in many industrial processes (cosmetics, pharmaceuticals, food industry). The role of the membrane is to protect the internal contents, to deliver them through capsule breakup under specific conditions, or to control mass transfer between the internal and external media. We consider here initially spherical liquid-filled capsules designed to be used in suspension in another liquid. As compared to a simple liquid droplet, the capsule has a more complex dynamic behaviour owing to the presence of the membrane that may buckle under compression or burst when the elastic tensions exceed a critical level.

There have been several numerical, experimental and theoretical studies of the deformation of a single capsule suspended in a flow. For example, the deformation of an isolated capsule freely suspended in a simple shear flow has been measured by Chang & Olbricht (1993) and by Walter, Rehage & Leonhard (2000, 2001) for different

membranes types. They find that after a short transient time, the capsule assumes a steady deformed profile oriented with respect to the far flow-field direction and that the membrane continuously rotates around this steady shape (*tank-treading* motion). However, in some cases, the membrane is found to fold at low shear rates (Walter *et al.* 2001). The motion of a capsule in shear flow has been modelled numerically with the boundary-integral method by Pozrikidis (1995) and by Ramanujan & Pozrikidis (1998) using a structured or an unstructured mesh, respectively. The orientation and deformation of the capsule can then be predicted as a function of flow strength and the rotational motion of the membrane is also recovered. Lac *et al.* (2004), using a structured mesh and a bi-cubic spline interpolation of the interface, have shown that stable equilibrium deformed shapes existed only between two limiting values of shear rate. For weak flows, the capsule buckles as observed experimentally; for high shear rates, the capsule exhibits high curvature tips and no equilibrium can be found.

In conclusion, if there are a number of results describing the motion of a single capsule in Stokes flow, such is not the case when there are two or more capsules interacting. Breyiannis & Pozrikidis (2001) modelled a two-dimensional suspension of capsules in simple shear flow for two surface fractions. They thus obtained a constitutive law for the two-dimensional suspension. However, the studies of a single capsule in shear flow all show that three-dimensional effects play an important role in determining the deformation and the tension distribution in the membrane. In particular, they are the cause of membrane buckling in certain conditions (Lac *et al.* 2004). Modelling a suspension of three-dimensional capsules is of course a difficult problem requiring large computer resources. As a first step, we tackle here the simpler situation where only two identical capsules interact in simple shear flow. The somewhat similar case of two interacting liquid droplets in simple shear flow has been modelled for low Reynolds and Weber numbers (thus excluding coalescence) by Loewenberg & Hinch (1997) and by Charles & Pozrikidis (1998), respectively, in three and two dimensions. They find that after the drops have crossed, there is an irreversible shift of their respective trajectories that depends on flow strength and on the viscosity ratio. An experimental study of the collisions of two droplets by Guido & Simeone (1998) has confirmed the results of the numerical model. Our objective is thus to investigate the role of the elastic membrane on this phenomenon. The capsule membrane obeys the neo-Hookean law and has no bending resistance. We find that in this case, the membranes may develop a buckling instability. In order to alleviate this problem, the capsules are first slightly prestressed by inflation, and the effect of such preinflation on the overall behaviour of the particles is discussed.

The main problem assumptions and equations are given in § 2. In § 3, we show how the numerical method developed by Lac *et al.* (2004) can be adapted to the problem of two identical capsules freely suspended in a simple shear flow. We will herein consider the case of two capsules with centres of mass located in the same shear plane, for this position corresponds to the strongest pairwise interaction. In this configuration, we investigate in § 4 the tensions exerted on the membranes and the centre trajectories for different capillary numbers and initial positions. In § 5, we discuss the relevance of the results, and necessary future work.

2. Problem statement

2.1. *Boundary integral formulation*

We consider two identical spherical capsules C_1 and C_2 with radius a, filled with a Newtonian fluid of viscosity μ and density ρ, and enclosed by a very thin hyperelastic

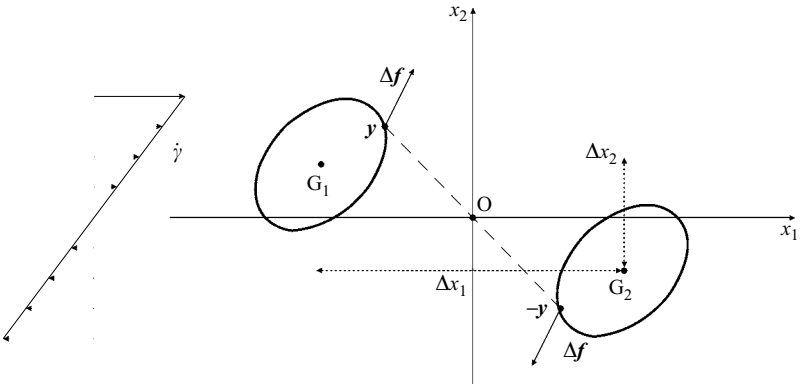

FIGURE 1. Representation of the relative position of the capsules in the shear plane (x_1, x_2).

membrane. The membrane is assumed to be a two-dimensional medium devoid of bending resistance and characterized by a surface shear modulus G_s and an area dilation modulus K_s. The two capsules are freely suspended in another Newtonian liquid with the same viscosity μ and density ρ and subjected to a simple shear flow with shear rate $\dot{\gamma}$ in the (x_1, x_2)-plane. The Reynolds number $\rho\dot{\gamma}a^2/\mu$ is assumed to be very small so that the motion of the internal and external fluids is governed by the Stokes equations. Assuming the same viscosity for the internal and external liquids allows us to simplify the fluid mechanics equations and thus facilitates the numerical procedure. This assumption is not too limiting, since it corresponds to a case where there is strong coupling between the internal and external flows.

Denoting the centres of mass of the capsules G_1 and G_2, we use a reference frame centred on the middle O of $\mathbf{G_1G_2}$ and moving with it (figure 1). In this reference frame, the undisturbed flow $\boldsymbol{u}^\infty$ of the external liquid is given by

$$u_1^\infty(\boldsymbol{x}) = \dot{\gamma}\, x_2, \quad u_2^\infty(\boldsymbol{x}) = u_3^\infty(\boldsymbol{x}) = 0. \tag{2.1}$$

The position of C_1 with respect to C_2 is given by the vector $\Delta\boldsymbol{x}$:

$$\Delta\boldsymbol{x} = \boldsymbol{x}(G_1) - \boldsymbol{x}(G_2) = 2\,\boldsymbol{x}(G_1). \tag{2.2}$$

The capsule centres G_1 and G_2 are initially located at position $\pm\Delta\boldsymbol{x}^0/2$. In the present study, Δx_1^0 and Δx_2^0 always have opposite signs, so that the capsules are naturally convected toward each other by the flow; by convention, we set Δx_1^0 to a negative value.

The fluid velocity at any point $\boldsymbol{x}$ can be expressed in terms of boundary integrals on the surfaces S_1 and S_2 of the two capsules (Pozrikidis 1992). When the internal and external fluid viscosities are equal, the integral equation takes the following simplified form with no contribution from the double-layer potential:

$$\boldsymbol{u}(\boldsymbol{x}) = \boldsymbol{u}^\infty(\boldsymbol{x}) - \frac{1}{8\pi\mu} \oint_{S_1 \cup S_2} \boldsymbol{J}(\boldsymbol{x}, \boldsymbol{y}) \cdot \Delta\boldsymbol{f}(\boldsymbol{y})\, \mathrm{d}S(\boldsymbol{y}), \tag{2.3}$$

where $\Delta\boldsymbol{f}$ represents the jump in viscous traction across the interfaces and $\boldsymbol{J}$ is the free space Green's function given in Cartesian coordinates by

$$J_{ij}(\boldsymbol{x}, \boldsymbol{y}) = \frac{\delta_{ij}}{r} + \frac{r_i\, r_j}{r^3}, \tag{2.4}$$

with $\boldsymbol{r} = \boldsymbol{y} - \boldsymbol{x}$ and $r = \|\boldsymbol{r}\|$.

Since the capsules are identical, their deformed shapes exhibit central symmetry with respect to O. Consequently, on two symmetric points $\boldsymbol{y}$ and $-\boldsymbol{y}$ taken on the surface of C_1 and of C_2, respectively, the load is $\Delta \boldsymbol{f}(\boldsymbol{y})$ and $\Delta \boldsymbol{f}(-\boldsymbol{y}) = -\Delta \boldsymbol{f}(\boldsymbol{y})$, respectively (figure 1). The integral equation (2.3) can thus be taken over only one capsule:

$$\boldsymbol{u}(\boldsymbol{x}) = \boldsymbol{u}^{\infty}(\boldsymbol{x}) - \frac{1}{8\pi\mu} \oint_{S_1} [\boldsymbol{J}(\boldsymbol{x}, \boldsymbol{y}) - \boldsymbol{J}(\boldsymbol{x}, -\boldsymbol{y})] \cdot \Delta \boldsymbol{f}(\boldsymbol{y}) \, \mathrm{d}S(\boldsymbol{y}). \tag{2.5}$$

2.2. *Membrane mechanics*

A detailed presentation of the mechanics of thin membranes may be found in a number of references (e.g. Barthès-Biesel & Rallison 1981; Pozrikidis 1995; Barthès-Biesel, Diaz & Dhenin 2002; Pozrikidis 2003, chap. 1 and 2) and is outlined only briefly here. Owing to its thinness, the membrane is treated as a two-dimensional hyperelastic surface with no bending resistance. The elastic stresses reduce to tensions $\boldsymbol{T}$ (forces per unit length of deformed surface lines) in the membrane plane.

The membrane equilibrium condition relates the load due to the jump of viscous traction across the interface to the membrane tension tensor $\boldsymbol{T}$

$$\nabla_s \cdot \boldsymbol{T} + \Delta \boldsymbol{f} = \boldsymbol{0}, \tag{2.6}$$

where ∇_s represents the surface gradient operator. A membrane material point at position $\boldsymbol{X}$ in the reference state is convected to position $\boldsymbol{x}$ at time t. A surface displacement gradient $\boldsymbol{A}$ is defined as

$$\boldsymbol{A} = (\boldsymbol{I} - \boldsymbol{nn}) \cdot \frac{\partial \boldsymbol{x}}{\partial \boldsymbol{X}} \cdot (\boldsymbol{I} - \boldsymbol{NN}), \tag{2.7}$$

where $\boldsymbol{N}$ and $\boldsymbol{n}$ denote the normal vectors to the membrane in the reference and in the deformed state, respectively, and $\boldsymbol{I}$ is the identity tensor. The surface Green-Lagrange deformation tensor is then given by

$$\boldsymbol{e} = \tfrac{1}{2} (\boldsymbol{A}^T \cdot \boldsymbol{A} - (\boldsymbol{I} - \boldsymbol{NN})). \tag{2.8}$$

We assume that the membrane material is isotropic in its plane, so that locally, the principal directions of strain and tension in the membrane plane are collinear. For simplicity, we denote those principal directions 1 and 2, keeping in mind that they should not be confused with the directions of flow. The deformation invariants are then defined by

$$I_1 = 2 \operatorname{tr} \boldsymbol{e} = {\lambda_1}^2 + {\lambda_2}^2 - 2, \quad I_2 = J_s^2 - 1, \tag{2.9}$$

where λ_1 and λ_2 are the principal extension ratios in the membrane plane, and $J_s = \lambda_1 \lambda_2$ the local surface area dilation. In order to close the problem, it is necessary to write a relation between the tension and the deformation of the membrane. In the case of a hyperelastic isotropic membrane, we may introduce a strain energy function W per unit of underformed membrane area, which is a function of the invariants, such that:

$$\boldsymbol{T} = \frac{2}{J_s} \frac{\partial W}{\partial I_1} \boldsymbol{A}^T \cdot \boldsymbol{A} + 2 J_s \frac{\partial W}{\partial I_2} (\boldsymbol{I} - \boldsymbol{nn}). \tag{2.10}$$

We assume here that each membrane consists in a thin sheet of a three-dimensional incompressible neo-Hookean material. In the limit of an infinitely thin membrane, the two-dimensional neo-Hookean law (see Barthès-Biesel *et al.* 2002) is given by

$$W = \frac{G_s}{2} \left(I_1 + 2 + \frac{1}{I_2 + 1} \right). \tag{2.11}$$

The principal tensions T_1 and T_2 in the membrane plane are then

$$T_1 = \frac{G_s}{\lambda_1 \lambda_2} \left(\lambda_1^2 - \frac{1}{\lambda_1^2 \lambda_2^2} \right), \tag{2.12}$$

with a similar expression for T_2, where the roles of indices 1 and 2 are exchanged. The surface Poisson ratio of such a membrane is $\nu_s = 1/2$, corresponding to an area dilation modulus $K_s = 3G_s$. ($K_s = (1+\nu_s)/(1-\nu_s)\, G_s$; an area incompressible membrane thus corresponds to $\nu_s = 1$.)

Finally, the no slip condition between the fluid and the membrane leads to the kinematic condition where for any point $\boldsymbol{x}$ on the interface, the fluid velocity is equal to the membrane velocity:

$$\boldsymbol{u}(\boldsymbol{x}) = \frac{\partial \boldsymbol{x}}{\partial t}(\boldsymbol{X}, t). \tag{2.13}$$

The overall deformation of the capsule is difficult to quantify. For a single capsule with a nearly ellipsoidal shape, the deformation is often measured by the Taylor parameter $D_{12} = (L_1 - L_2)/(L_1 + L_2)$ where L_1 and L_2 represent the length and breadth of the deformed profile in the shear plane. Here, since the capsules exhibit complex shapes, we chose to evaluate their deformation through the relative change of the surface area $\Delta A/A_s = A/A_s - 1$, where $A_s = 4\pi a^2$ is the initial membrane surface area and A the deformed area.

An important parameter is the elastic capillary number,

$$\varepsilon = \frac{\mu a \dot{\gamma}}{G_s}, \tag{2.14}$$

which measures the relative importance of the viscous stress exerted by the fluids compared to the elastic resistance of the membranes. This parameter may also be viewed as a non-dimensional measurement of shear rate for a given pair of capsules.

2.3. *Membrane buckling*

Neglecting bending resistance implies that the membrane must be under tension to be stable. Buckling instabilities appear when one of the two principal tensions becomes negative. As discussed by Lac *et al.* (2004), the post-buckling behaviour of the capsules cannot be captured since our membrane model does not account for bending resistance. However, the onset of buckling can be detected by the apparition of compressive stress followed by oscillations of different quantities (normal load, curvature, etc.) on the surface.

Lac *et al.* (2004) have studied the deformation of an isolated capsule suspended in simple shear flow and found that there were always compressive principal tensions in the membrane for small enough shear rates, such that $\varepsilon < \varepsilon_L$. As the shear rate increases, the membrane deformation and subsequent area dilation also increase and the tensions in the membrane become all positive. The capsule deformation is then stable. However, for large shear rates such that $\varepsilon > \varepsilon_H$, no equilibrium state seems to exist and the capsule is assumed to burst owing to continuous elongation. The values of ε_L and ε_H depend on the membrane constitutive law.

A way to eliminate the low shear buckling instability without introducing bending resistance is to prestress the capsule by means of an internal pressure that could be due, for example, to osmotic pressure if the membrane is semi-permeable (Sherwood *et al.* 2003). As shown by Lac & Barthès-Biesel (2005), this creates an initial isotropic tension T_0 that depends on the initial inflation ratio $\alpha = a/a_0 - 1$, where a and a_0 denote the radius of the capsule after and before inflation, respectively. In particular,

for a neo-Hookean membrane, T_0 is obtained from (2.12) with $\lambda_1 = \lambda_2 = 1 + \alpha$. Thus, in the limit of small inflation, $T_0 = 6\alpha G_s$. Lac & Barthès-Biesel (2005) also showed that for a preinflated capsule, there was still a maximum shear rate ε_H above which no equilibrium could be found. The only effect of prestressing is to increase slightly the value of ε_H.

In equation (2.14) as well as in the rest of the paper, the chosen reference length is the inflated capsule radius a, rather than the unstressed capsule radius a_0. Indeed, the inflated radius a is the proper length scale of the flow problem. Besides, it is easier to measure than a_0.

3. Numerical method

Using the boundary-element method and Lagrangian interface tracking, Lac *et al.* (2004) developed a numerical model of the motion and deformation of an isolated capsule in shear flow. We have adapted this model to the present problem of two capsules.

The two undeformed, but eventually pre-inflated, capsules are placed in the suspending liquid with their centres G_1 and G_2 at initial positions $\pm\Delta\boldsymbol{x}^0/2$, respectively. At time $t = 0$, we start the simple shear flow (2.1) and follow the capsule motion and deformation in time. At any given time t, we thus know the displacement of the membrane material points and can then compute the displacement gradient $\boldsymbol{A}$, the deformation tensor $\boldsymbol{e}$ and the elastic tensions $\boldsymbol{T}$ in the membrane from equations (2.7) to (2.11). The load $\Delta\boldsymbol{f}$ on the membrane follows from (2.6). The integral equation (2.5) yields the new velocity of the capsule membrane points. The position of the membrane at time $t + \Delta t$ is then updated by means of an explicit fourth-order Runge–Kutta integration of the kinematic equation (2.13) and the process is repeated. Since we use an explicit time scheme, the time step Δt must be very small to ensure numerical stability. The procedure is stopped manually when the capsules have crossed over and when the x_2-coordinate of the centres of mass has become constant in time.

Following Lac *et al.* (2004), the position of any point $\boldsymbol{x}$ on the interface is determined by two independent curvilinear coordinates θ^1 and θ^2 which initially correspond to the azimuthal and meridional angles in spherical coordinates. The initial surface is then tessellated with $n \times m$ elements, corresponding to n and m equal intervals in the θ^1 and θ^2 directions, respectively. The intersection of parallel curve i and meridian curve j defines the grid node $\boldsymbol{x}_{ij}$. Since the surface is holomorphic to a sphere, the mesh contains two poles at $\theta^1 = 0, \pi$.

The use of a structured mesh allows us to interpolate the surface by means of bi-cubic B-splines:

$$\boldsymbol{x}(\theta^1, \theta^2, t) = \sum_{k,l} \tilde{\boldsymbol{x}}_{kl}(t)\, B_k^n(\theta^1)\, B_l^m(\theta^2), \tag{3.1}$$

where B_k^n and B_l^m are basis piecewise cubic polynomials, and $\tilde{\boldsymbol{x}}_{kl}$ are the spline coefficients associated to $\boldsymbol{x}$ at time t. For each scalar variable (e.g. each component of $\boldsymbol{x}$), a total of $(n+3) \times (m+3)$ spline coefficients are required. This procedure ensures continuity up to second order of the metric properties of the capsule surface. The integral in (2.5) is calculated with the Gauss quadrature technique. Owing to the definition of the kernel $\boldsymbol{J}$, the velocity computed in (2.5) is divergence-free for any surface force distribution $\Delta\boldsymbol{f}$. A way to measure the accuracy of the integration procedure combined with the spline representation of the surface is thus to check the

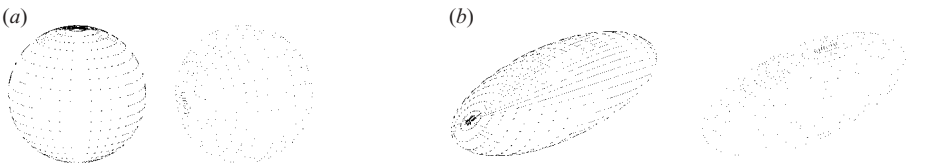

FIGURE 2. The two-grid method: the surfaces in solid lines show the actual Lagrangian grid (a) at $t=0$ and (b) at time t. The dotted line surfaces show the secondary grid, initially created from a $\pi/2$ rotation of the pole axis, and deduced from the deformed shape at time t.

volume conservation of the capsule during deformation. In all our simulations, the maximum relative volume change ever observed was typically 10^{-4} for 20×40 grids and 10^{-6} for 30×60 grids.

The dominant error of the numerical scheme comes from the determination of $\Delta \boldsymbol{f}$, because equation (2.6) is singular at the two grid poles. In the case of an isolated capsule in shear flow, the pole value of the load may be extrapolated (Lac *et al.* 2004; Lac & Barthès-Biesel 2005). Since the steady capsule deformation is obtained rapidly after a limited number of iterations, the extrapolation procedure does not create a large error. Indeed, the method has been validated by comparison with other numerical results obtained with an unstructured mesh (e.g. Ramanujan & Pozrikidis 1998). However, the crossing of two capsules is a transient process that requires long computation times. Then, if the pole value of the load is extrapolated, the accumulated error in the vicinity of these points may become large and eventually cause the numerical scheme to diverge after long computation times.

We have thus developed a new method to calculate the load on the surface with high accuracy. The idea is to describe the capsule surface with two grids where the pole axes are initially orthogonal (figure 2a). Grid 1 corresponds to the one described above. Grid 2 corresponds to a similar $n\times m$ partition of the initial surface, but with poles located on points $\theta^1=\pi/2$; $\theta^2=0,\pi$ of grid 1. Each node of the secondary grid has associated coordinates (θ^1,θ^2) on the primary grid. At each time step, we use these coordinates in (3.1) to determine the position of the nodes of grid 2 on the deformed surface (figure 2b), and then repeat the load computation (2.6) on grid 2. This procedure gives us two load distributions $\Delta \boldsymbol{f}^{(1)}$ and $\Delta \boldsymbol{f}^{(2)}$, corresponding to grids 1 and 2 where the respective poles have been excluded. We then calculate the final load as

$$\Delta \boldsymbol{f} = \omega\, \Delta \boldsymbol{f}^{(1)} + (1-\omega)\, \Delta \boldsymbol{f}^{(2)}, \tag{3.2}$$

where $\omega(\theta^1,\theta^2)$ is a weight function going to zero at the poles of grid 1 and to unity at the poles of grid 2. Since the singularity in equation (2.6) behaves as $\sin^{-2}\theta^1$ in the vicinity of $\theta^1=0,\pi$ when the capsule is spherical, we have chosen $\omega=\sin^2\theta^1$.

As a validation of this method, we have compared the results obtained with one and two grids for a single capsule in simple shear flow. Figure 3 shows the Taylor deformation in the shear plane D_{12} *vs.* time for $\varepsilon=0.0375$ and different prestress levels. These parameters correspond to difficult cases because the capillary number is very small, and the numerical scheme is extremely sensitive to accumulated errors. The gain of stability provided by the present method is obvious; after steady state has been reached, the single-grid method exhibits some slow oscillations (which eventually lead to numerical instability after long times), whereas the two-grid method reaches a very stable plateau.

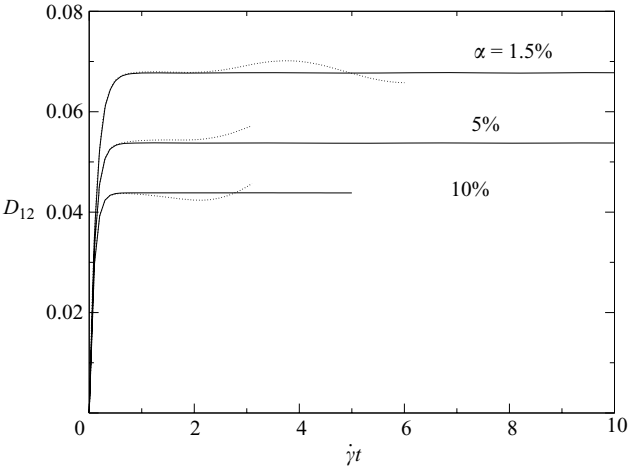

FIGURE 3. Deformation of a single capsule in simple shear flow in time for $\varepsilon = 0.0375$ and different values of α; comparison between the single-grid method (dotted lines) and the two-grid method (solid lines).

In the result presented hereinafter, most of the simulations were performed with a 20×40 grid. When the capsule shape exhibited high curvatures or when extra-precision was required, the mesh was refined to a 30×60 grid. Grids with 10×20 and 40×80 elements were also used, but for convergence tests only.

4. Interaction of two capsules in the same shear plane

In order to assess the relative importance of hydrodynamic interaction effects, it is of interest to compare the relevant quantities found for two capsules to those obtained for a single capsule in shear flow without (Lac *et al.* 2004) or with preinflation (Lac & Barthès-Biesel 2005). These quantities will be denoted by the superscript (*sc*).

At the start of flow, the capsules are undeformed and their centres G_1 and G_2 are initially placed in the same shear plane (i.e. $\Delta x_3^0 = 0$) and separated by $(\Delta x_1^0, \Delta x_2^0) = (-8a, 0.5a)$, except in §4.5 where the effect of initial separation is specifically studied. Although the capsules are free to move in space, we find that $|\Delta x_3(t)/a|$ remains smaller than 10^{-12} typically, which demonstrates the stability of this configuration.

4.1. *Effect of prestress*

We consider the case $\varepsilon = 0.45$, a value for which a single capsule reaches a steady deformation even when the membrane is initially unstressed ($\alpha = 0$), and study the effect of preinflation ratios $\alpha = 0, 2.5, 5, 10\%$. Since $\Delta x_2^0 > 0$, the capsules are naturally convected towards each other by the flow. Figure 4(*a*) shows the evolution of the relative area dilation of each capsule $\Delta A/A_s$ as a function of position $\Delta x_1/2a$ of the centre of mass G_1 for different values of α. Note that since the length scale is the inflated capsule radius, the initial value of $\Delta A/A_s$ is zero for all preinflation ratios. For comparison purpose, the steady area increase for a single capsule $\Delta A^{(sc)}/A_s$ is also shown in the figure (dotted lines). When the capsules overpass ($\Delta x_1 \approx 0$), $\Delta A/A_s$ reaches a maximum value significantly higher than that observed for a single particle at the same inflation. The relative area dilation increase goes from 40% when $\alpha = 0$ to 70% when $\alpha = 10\%$. Once they have passed each other ($\Delta x_1 > 0$), the capsules

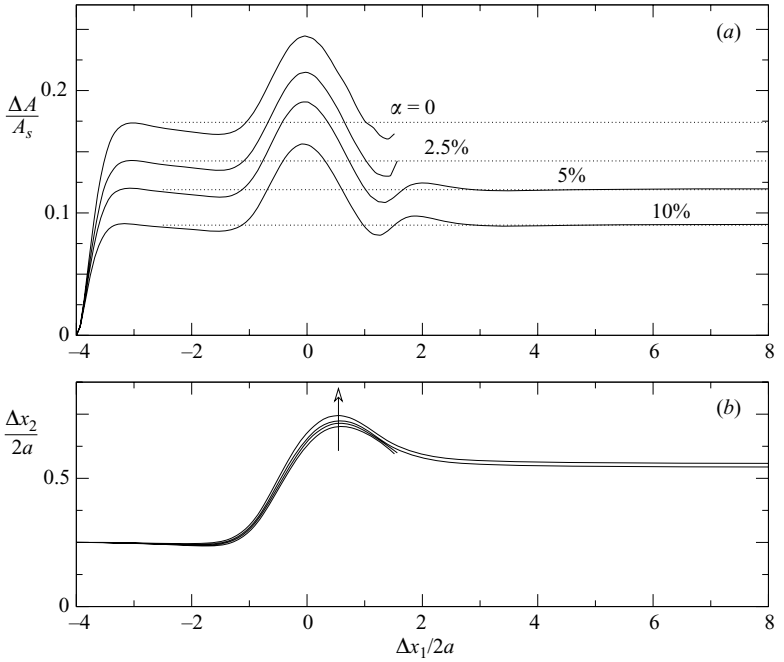

FIGURE 4. (*a*) Relative area dilation as a function of the centre position $x_1(\mathrm{G}_1) = \Delta x_1/2a$. Dotted lines show the steady value for a single capsule. (*b*) Trajectory of centre G_1 for $\alpha = 0, 2.5\%, 5\%, 10\%$ ($\varepsilon = 0.45$, $\Delta x_1/2a^0 = -4$, $\Delta x_2^0/2a = 0.25$). The horizontal axis is the same for (*a*) and (*b*).

undergo a visco-elastic relaxation due to coupling between membrane elasticity and fluid viscosity and they finally reach a steady state for $\Delta x_1/2a > 3.5$, approximately. Since the steady deformation is the same as that observed for a single capsule, this means that the capsules do not interact any more. As already observed for a single capsule, one effect of prestress is to decrease capsule deformation or equivalently, area dilation ΔA. However, it was not possible to follow the complete crossing of the capsules for $\alpha = 0\%$ and $\alpha = 2.5\%$ owing to the appearance of compressive stresses in the membranes during the relaxation phase after the capsules have passed each other. This point will be addressed in detail in § 4.4.

The trajectory of the centre G_1 of capsule 1 is shown in figure 4(*b*) for different values of α. We observe an irreversible trajectory shift across streamlines since capsule separation Δx_2 at steady state is greater than the initial value Δx_2^0. We also note that the effect of the membrane prestress on the capsule centre trajectories is rather weak.

In order to capture the complete crossing process of two capsules, we have set the preinflation ratio to $\alpha = 5\%$ in all the results presented hereinafter. For neo-Hookean membranes, this value corresponds to a prestress $T^0 \approx 0.254\, G_s$ and a maximum capillary number $\varepsilon_H \approx 0.805$.

4.2. *Detailed analysis of the crossing process*

The hydrodynamic interaction of the two capsules is now studied in detail for two values of capillary number $\varepsilon = 0.075$ and $\varepsilon = 0.45$ corresponding to low and fairly high shear rates. The inflation ratio is set to 5% and the initial cross-flow separation $\Delta x_2^0/2a$ to 0.25. The deformed shape of a single capsule is symmetrical with respect to its centre. Thus, the appearance of profile asymmetry coincides with the onset

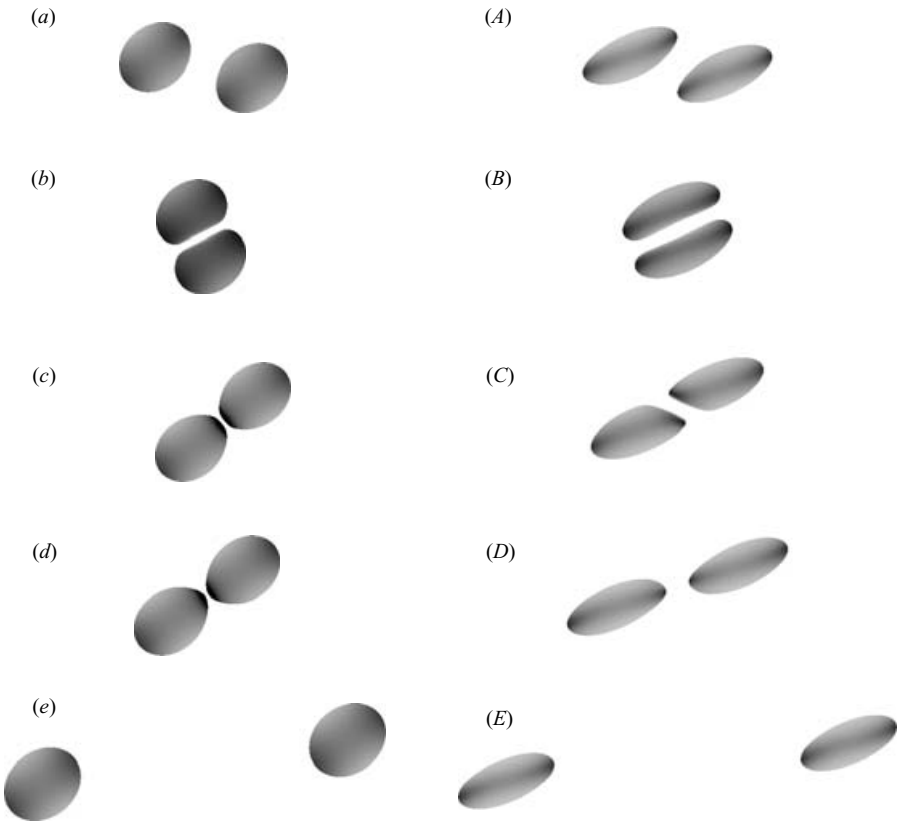

FIGURE 5. Sequence showing, from top to bottom, the motion of the capsules for $\Delta x_2^0/2a = 0.25$ and $\alpha = 0.05$; (*a*–*e*) $\varepsilon = 0.075$, $\Delta x_1^0/2a = -4$; (*A*–*E*) $\varepsilon = 0.45$, $\Delta x_1^0/2a = -5$. The grey mapping corresponds to the normal load $\Delta \boldsymbol{f} \cdot \boldsymbol{n}$.

of hydrodynamic interactions between two capsules. The corresponding sequences of capsule shapes are shown in figure 5. When $\Delta x_1/2a \approx -1.5$, the capsules start to interact and their shapes are no longer exactly symmetrical with respect to their centres of mass (figure 5*a*, *A*). As separation decreases ($-1.5 \leqslant \Delta x_1/2a \leqslant 0$), the centres of mass are shifted across streamlines and parts of the membranes flatten (figure 5*b*, *c*) or become concave (figure 5*B*, *C*). After crossing ($\Delta x_1 > 0$), the capsules are convected away from each other and the membranes recover a convex shape (figure 5*d*, *D*). For large separations $\Delta x_1/2a > 3.5$, the hydrodynamic interaction between the particles is no longer visible and both capsules have relaxed to the steady deformed shape obtained for a single capsule subjected to the same flow conditions (figure 5*e*, *E*).

In order to understand better the hydrodynamics of crossing, it is useful to compute the pressure p_0 at the flow centre ($\boldsymbol{x} = \boldsymbol{0}$), given by

$$p_0 - p^\infty = -\frac{1}{4\pi} \oint_{S_1} \frac{\Delta \boldsymbol{f}(\boldsymbol{y}) \cdot \boldsymbol{y}}{\|\boldsymbol{y}\|^3} \, \mathrm{d}S(\boldsymbol{y}), \tag{4.1}$$

where p^∞ denotes the far field pressure. In figure 6, we have plotted the pressure difference $p_0 - p^\infty$ as a function of capsule separation Δx_1 for the two values of capillary number. High positive pressures occur during crossing ($-1 \leqslant \Delta x_1/2a \leqslant 0.5$, approximately) when the two capsules are separated by a thin lubrication film, as

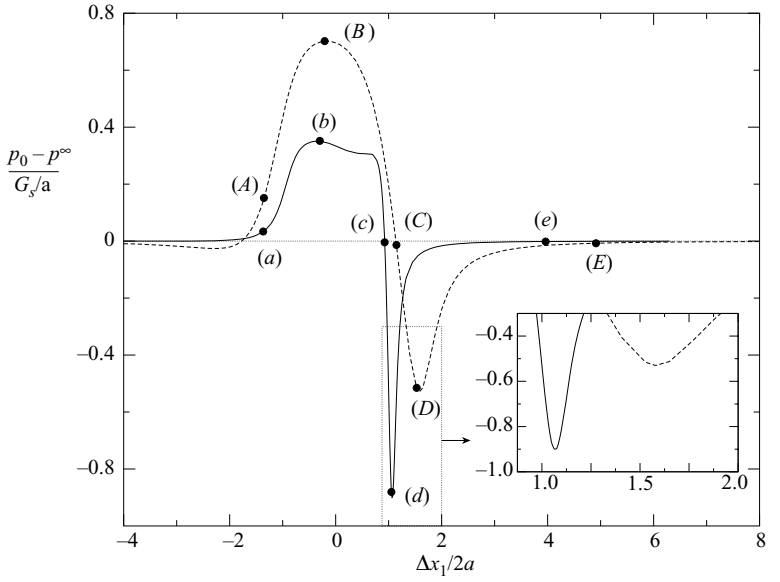

FIGURE 6. Pressure p_0 as a function of centre position $x_1(\mathrm{G}_1) = \Delta x_1/2a$. The same flow conditions as in figure 5. Symbols ● correspond to the sequences in figure 5. During separation, the pressure is continuous (inset) and its sharp variation is due to the combined effects of film thickness increase and membrane elastic recoil. - - -, $\varepsilon = 0.045$; —, 0.075.

FIGURE 7. Magnified cross-views of figures 5(*b*) and 5(*B*) (left and right). The two capsules (C_1 above, C_2 below) are artificially cut in half to give a clear view of the membrane in the film region.

shown in figure 5(*b*, *B*), and in more detail in figure 7. The increase in film pressure corresponds to the squeezing of the lubrication film. The high external pressure in the film leads to large deformations where the membranes flatten or even become concave (figure 7), depending on the value of the capillary number. Furthermore, large curvatures appear at the edge of the film. When the capsules separate ($\Delta x_1/2a \approx 1$), the combined effects of film thickness increase and membrane elastic recoil lead to a fast decrease in pressure that becomes negative (figure 6*c*, *d*, *C*, *D*) and then stablilizes to zero after the capsules have separated (figure 6*e*, *E*). This leads to transient asymmetric capsule shapes with high curvature tips in the separation region as apparent in figure 5(*d*, *D*). A similar phenomenon was observed experimentally for drops (Guido & Simeone 1998, figure 5). Furthermore, the suction in the lubrication film creates a drag force on the capsules with a non-zero x_2-component (negative for C_1, positive for C_2), which reduces the cross-flow separation Δx_2 during the parting

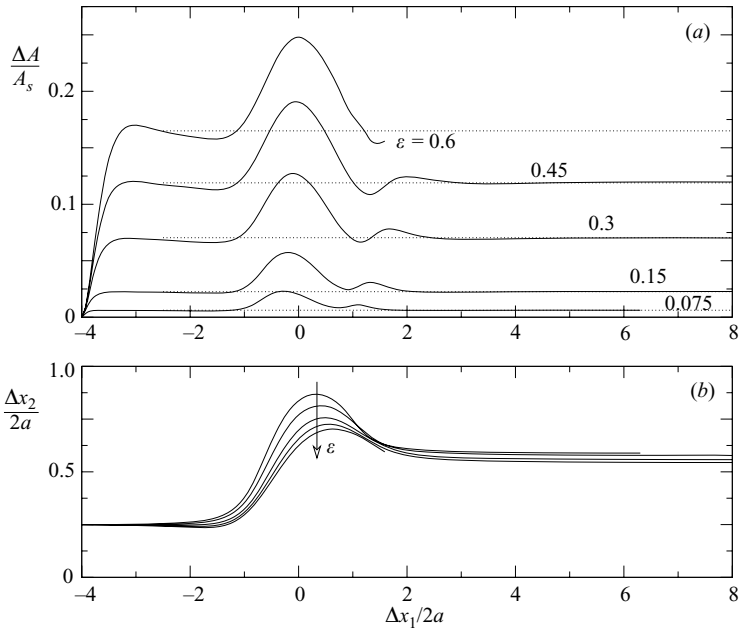

FIGURE 8. (*a*) Area dilation as a function of centre position $\Delta x_1/2a$; dotted lines show the steady value for a single capsule; (*b*) trajectory of centre G_1; $\alpha = 0.05$, $\Delta x_1^0 = -8a$, $\Delta x_2^0 = 0.5a$.

phase. A similar phenomenon was observed experimentally for drops (Guido & Simeone 1998, figure 5).

The high membrane deformation is obviously coupled to an important local increase of the elastic stress level that may cause material damage, as investigated in the next section.

4.3. *Effect of capillary number*

We now study the global effect of capillary number when the inflation ratio is set to 5% keeping the same initial position of the undeformed capsule centres of mass $(-8a, 0.5a)$. The relative area increase and centre of mass trajectory are shown in figure 8 for set values of ε. The same phenomena as described in § 4.1 are recovered here. Since each capsule represents a greater obstacle for the other when ε decreases, the maximum deviation increases as ε drops from 0.6 to 0.075 (figure 8*b*). For all capillary numbers, we note a significant increase of area dilation during cross over when $\Delta x_1 \approx 0$ (figure 8*a*). The viscoelastic relaxation to the single-capsule equilibrium shape occurs only for moderate values of ε. For $\varepsilon \geqslant 0.6$, it was not possible to capture the complete separation phase owing to the occurrence of buckling effects in the membrane. This point will be discussed in detail in the next section.

The increase in deformation leads to an increase in elastic tensions in the membrane, which can be measured by the value of the maximum principal elastic tension T_{max} for a given deformed state of the capsule. Figure 9 shows, for different capillary numbers, the evolution of T_{max} as a function of centre separation Δx_1. The value of the maximum tension $T_{max}^{(sc)}$ for a single capsule is also shown. We note a first peak of tension during crossing where the extra tension $T_{max} - T_{max}^{(sc)}$ ranges from 24% to 12% of $T_{max}^{(sc)}$ when ε varies from 0.075 to 0.45. The relative decrease of extra tension when ε increases should not be surprising. Indeed for fixed flow conditions, increasing ε means increasing the membrane ability to deform. Here, a significant

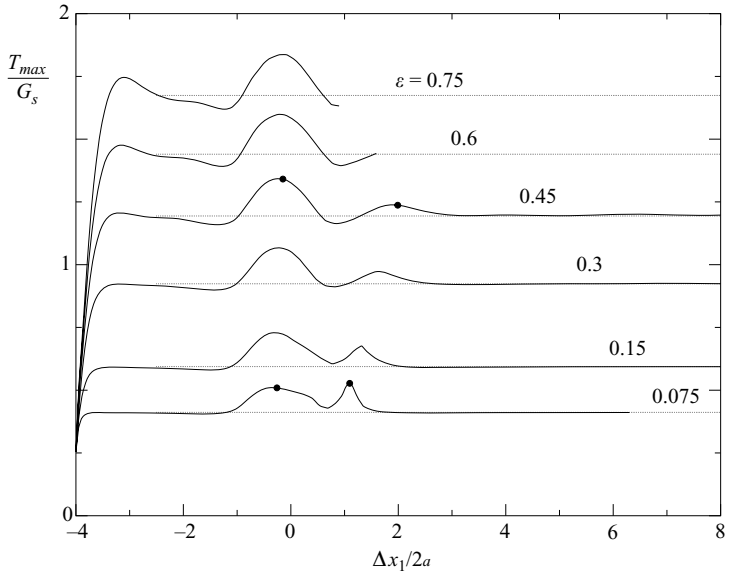

FIGURE 9. Maximum principal tension in the membranes as a function of Δx_1 for different capillary numbers and for $\Delta x_1^0/2a = -4$, $\Delta x_2^0/2a = 0.25$. Dotted lines show the value of $T_{max}^{(sc)}$ for a single capsule; symbols ● correspond to the four profiles shown in figure 10.

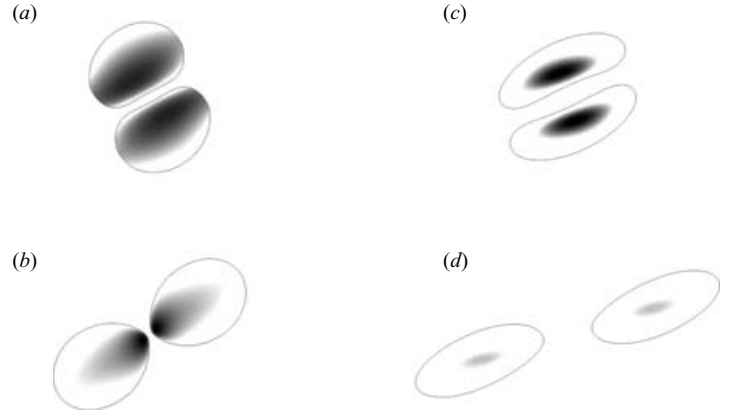

FIGURE 10. Deformed profiles of the capsules at times when the maximum tension in the membranes reaches high values. The grey level shows the locations where one of the principal tensions exceeds $T_{max}^{(sc)}$; (*a*, *b*) $\varepsilon = 0.075$; (*c*, *d*) $\varepsilon = 0.45$.

increase in deformation (figure 8a) leads to a moderate increase in tension, because the membrane obeys a neo-Hookean constitutive law which is strain softening under large deformation (Barthès-Biesel *et al.* 2002). Had we assumed a strain hardening law such as that of Skalak *et al.* (1973), we would expect to find significantly higher stresses in the membranes for the same deformation level and a possible increase of the extra tension with ε.

The maximum tension also varies during the separation process and T_{max} fluctuations can be as large as the initial peak. It is interesting to locate the areas where the largest elastic stresses occur. We thus show the distribution of maximum

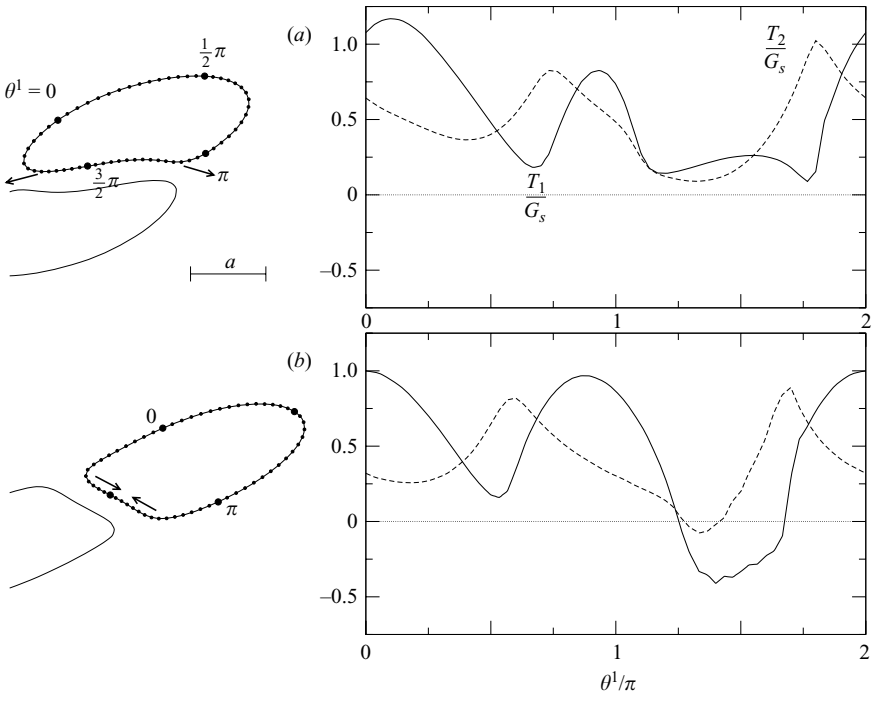

FIGURE 11. Principal elastic tensions T_1 and T_2 along the $x_3 = 0$ profile at large capillary number ($\varepsilon = 0.6$, $\alpha = 0.05$). Arrows show qualitatively the direction of T_1; (*a*) $\Delta x_1/2a \approx 0.54$; (*b*) $\Delta x_1/2a \approx 1.27$.

principal tensions on the capsule profiles at the first and second overshoots in figure 9, for $\varepsilon = 0.075$ and $\varepsilon = 0.45$. The grey-level mapping represents the value of the ratio $T_{max}/T_{max}^{(sc)}$ with a cutoff value at unity. For an isolated capsule, the maximum tension occurs in the equatorial region of the deformed shape. During crossing, the maximum tension location is roughly the same as when the capsule is alone. This means that the extra-tension in the membranes of interacting capsules is due to the extra-elongation during the crossing. During separation however, two different processes appear, depending on the value of ε. For relatively large capillary numbers ($\varepsilon \geqslant 0.3$, typically), the second tension overshoot is weak compared to the first and is located in the same area as for a single capsule, indicating that it is simply due to shape oscillation. For small capillary numbers, e.g. $\varepsilon = 0.075$, a stress concentration located at the tips of the capsules appears when the depression caused by separation is maximum. This is due to the thinning of the separating film as the capsule deformability decreases, leading to a stronger interaction between the particles.

In conclusion, hydrodynamic interactions increase the stress level in the membrane and may lead to burst, even when viscous stresses are not high enough to break a single isolated capsule.

4.4. *Buckling instabilities due to hydrodynamic interactions*

We now investigate the problem of membrane buckling that occurs during crossing for large capillary numbers or low inflation rates. As an example, we consider the case $\alpha = 0.05$, $\varepsilon = 0.6$, and $\Delta x_2^0/2a = 0.25$. In figure 11, we show the two principal tensions T_1 and T_2 in the membrane along the profile located in the shear plane (x_1, x_2), as a

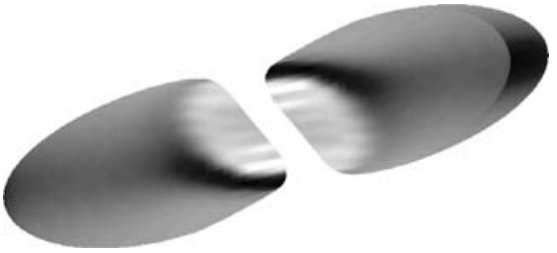

FIGURE 12. Wrinkling of the membranes in the flattened film region owing to flexion instabilities; $\varepsilon = 0.6$, $\alpha = 0.05$, when $\Delta x_1/2a \approx 1.27$ (same as figure 11*b*).

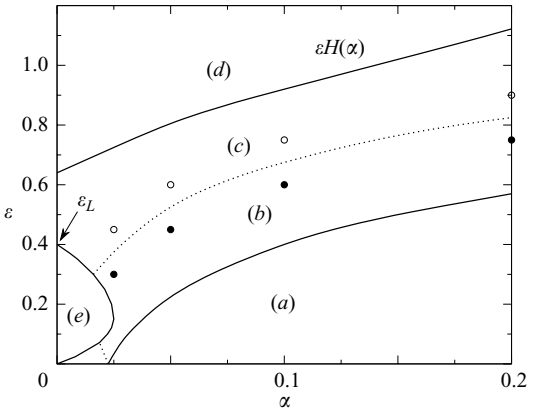

FIGURE 13. Stability diagram for $\Delta x_2^0/2a = 0.25$; (*a*) stable zone, where no compression occurs during motion; (*b*) small compression occurs, but the instability does not develop and the capsules overlap; (*c*) compression instability develops and the method diverges (e.g. figure 12); (*d*, *e*) zones where a single capsule in simple shear flow is unstable. ●, the last case when the capsules could cross; ○, the first failed case.

function of curvilinear coordinate θ^1 which varies between 0 and 2π along that line. Principal tension T_1 is tangent to this profile while T_2 is orthogonal to the shear plane.

For $\Delta x_1/2a \approx 0.54$ (figure 11*a*), the capsules have begun crossing over and the membranes are stretched everywhere (although the figure shows tensions only in the shear plane) because the capillary number and the membrane prestress are large enough. As the capsules are convected away from each other ($\Delta x_1/2a \approx 1.27$), the lubrication film pressure decreases (see figure 6) and the membranes tend to evolve from concave to convex shapes. During this process, compression takes place in the θ^1-direction (figure 11*b*). Consequently, membrane folds tend to develop in the direction orthogonal to the shear plane (figure 12). For the same capillary number, the phenomenon disappears when α is increased to 0.1, for example, because the stress level in the membranes is globally increased. However, for $\alpha = 0.1$, the same instability is found again for higher values of ε.

Figure 13 shows a stability diagram in the (α, ε)-plane for initial separation $\Delta x_2^0/2a = 0.25$. There are two instability regions denoted (*d*) and (*e*). Zone (*d*) is bounded by the curve $\varepsilon = \varepsilon_H(\alpha)$ above which there are no equilibrium capsule shapes as described by Lac & Barthès-Biesel (2005). In zone (*e*), the equilibrium shapes are unstable and membrane folds tend to appear around the capsule equator, as

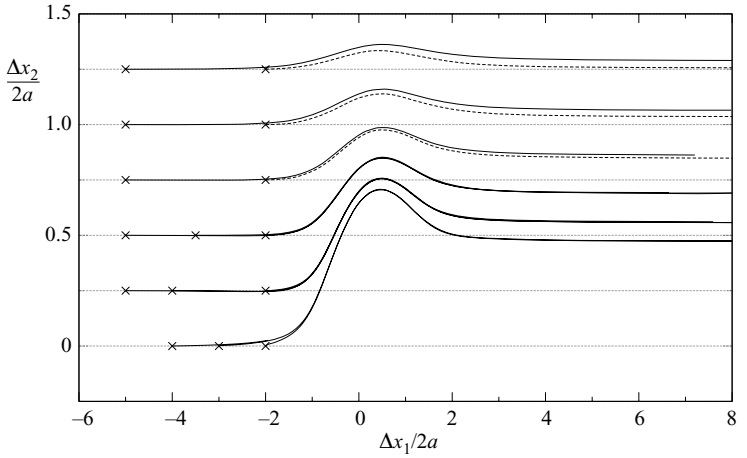

FIGURE 14. Trajectory of capsule 1 for different initial positions $(\Delta x_1^0, \Delta x_2^0)$ and for $\varepsilon = 0.3$, $\alpha = 0.05$; $\times$, initial position of G_1. A small value of $|\Delta x_1^0|/2a$ may influence the trajectory for high values of $\Delta x_2^0/2a$, because the capsules are convected too fast to reach steady deformation before they start interacting (dashed trajectories).

observed experimentally by Walter *et al.* (2001) and predicted numerically by Lac & Barthès-Biesel (2005).

Elsewhere (zones a, b, c), a single capsule is stable, but instabilities may arise from hydrodynamic pairwise interactions. Zone (a) corresponds to a stable region for two interacting capsules, where all principal tensions are greater than or equal to zero during motion. In zone (b), some negative tensions appear as the capsules cross, but they are too small and occur on too short a time scale to let the instability develop, so that it is possible to follow the complete crossing of the capsules. Zone (c), however, corresponds to larger compressions which lead to buckling instability during the separation phase (see for example figure 12). As the border between zones (b) and (c) is not precise, it was drawn with a dotted line in figure 13. When both ε and α are small – small triangular zone below (e) –, the compression instability sets in during the collision process, i.e. before the capsules have crossed.

As Δx_2^0 increases, stability zone (a) expands to higher values of ε for a given α and zones (b) and (c) shrink accordingly. In the limit $\Delta x_2^0/2a \to \infty$, the capsules do not interact and the upper limit of region (a) is the curve $\varepsilon_H(\alpha)$.

4.5. *Effect of the initial position, trajectory shift*

As shown in figures 4(b) and 8(b), the capsules deviate irreversibly from their original trajectory after they have crossed. This trajectory shift is due to deformability and viscous flow inside and outside the capsule, since no such final crossflow displacement occurs with rigid spheres (Batchelor & Green 1972; Van de Ven & Mason 1976). For liquid drops, a similar trajectory shift has also been found numerically by Loewenberg & Hinch (1997) and observed experimentally by Guido & Simeone (1998).

We characterize the trajectory of the capsules with three parameters: the initial, maximum and final centre separations, respectively denoted Δx_2^0, Δx_2^m and Δx_2^∞. The effect of the initial positions of the centres on the capsule trajectories is shown in figure 14 for $\varepsilon = 0.3$. The value of $\Delta x_2^0/2a$ determines the relative convection velocity of the two capsules. For $\Delta x_2^0/2a = 0$, there is *a priori* no relative centre velocity imposed by the undisturbed flow and thus when the capsules are very far apart

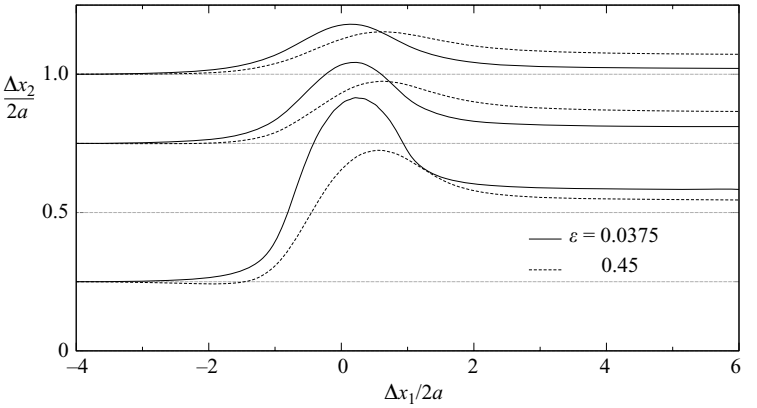

FIGURE 15. Comparison of trajectories for large and small capillary numbers and different initial positions.

($|\Delta x_1^0|/2a \gg 1$), they should not have any relative motion. However, the *tank-treading* rotation of the capsule membrane around the steady deformed profile creates a three-dimensional disturbance flow that vanishes as a/r, where r is the distance measured from one capsule centre. Consequently, for capsules as far apart as $\Delta x_1^0/2a \approx -4$ (in the cases considered here), this weak disturbance flow tends to move the capsule centres off the x_1-axis and eventually leads to crossing, as is apparent in figure 14 for $\varepsilon = 0.3$. For $\Delta x_1^0/2a < -3$, we did not follow the complete crossing because the relative motion of the capsules is extremely slow. For example, for $\Delta x_1^0/2a = -4$, it takes a dimensionless time $\dot{\gamma} t = 100$ to reach $\Delta x_1/2a \approx -2$. Nevertheless, it seems that all the computed trajectories converge to the same path.

For $\Delta x_2^0 > 0$, a study of the influence of position Δx_1^0 along the flow axis indicates that the trajectories are independent of Δx_1^0 if the capsules have reached a steady deformed state before they start interacting. In figure 14 we show that values of $|\Delta x_1^0|/2a > 2$ have hardly any incidence on the capsule trajectory shift, provided $\Delta x_2^0/2a$ is not too large. When $\Delta x_2^0/2a$ is large, the capsules are convected towards each other with a large velocity ($\sim \dot{\gamma}\, \Delta x_2^0$) and thus $|\Delta x_1^0|/2a$ has to be large enough for the capsules to have time to reach a steady deformation before crossing. The dashed trajectories in figure 14 correspond to situations where $|\Delta x_1^0|/2a$ is not large enough for the chosen value of $\Delta x_2^0/2a$ and where the capsules are not completely deformed when they start interacting. Except for the above short study, all the results presented in this paper were obtained with values of $|\Delta x_1^0|/2a$ large enough for this parameter to have no effect whatsoever.

Finally, we note on figure 14 that the maximum $\Delta x_2^m - \Delta x_2^0$ and final $\Delta x_2^\infty - \Delta x_2^0$ deviations decrease as separation increases. For $\Delta x_2^0/2a > 1.25$, there is essentially no trajectory shift.

The centre trajectories also depend on ε, i.e. on capsule deformability, as shown in figure 15 for $\varepsilon = 0.0375$ and 0.45. For given flow conditions, the smaller value of ε corresponds to the less deformable capsule. As expected, we find that the maximum deviation $\Delta x_2^m - \Delta x_2^0$ increases as ε and Δx_2^0 decrease. This means that the less deformable particles have to deviate more as they cross. Furthermore, since membrane prestress decreases capsule deformability, we also find that $\Delta x_2^m - \Delta x_2^0$ increases with inflation ratio α (figure 4). For large initial offsets, the maximum deviation $\Delta x_2^m - \Delta x_2^0$ becomes less sensitive to capillary number. However, as ε increases, it occurs for larger

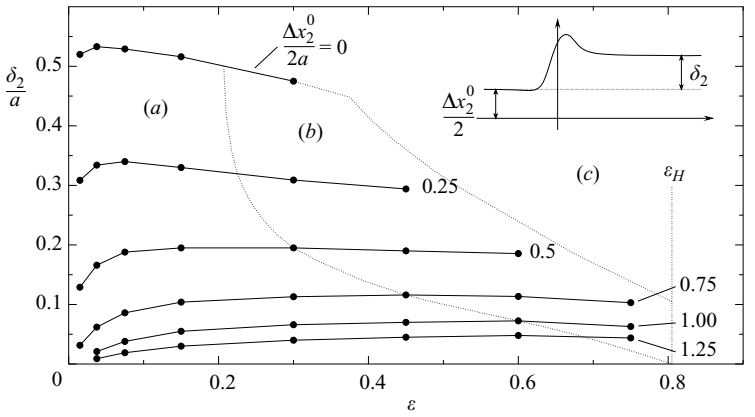

FIGURE 16. Final deviation of capsule C_1 as a function of ε, for $\alpha = 5\%$ and different initial positions $\Delta x_2^0/2a = 0$, [0.25], 1.25. The dotted lines show the limits of the stability region as $\Delta x_2^0/2a$ increases, with the same notations (a, b, c) as in figure 13. Inset: schematic of the trajectory of centre G_1.

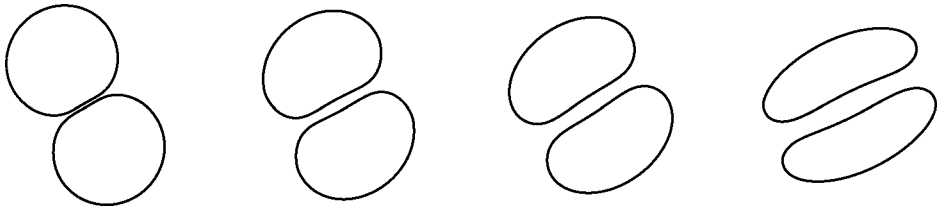

FIGURE 17. Evolution of the viscous film between the capsules as ε increases ($\Delta x_2^0/2a = 0.25$ and, from left to right, $\varepsilon = 0.015; 0.075; 0.15; 0.45$).

values of Δx_1, because the capsules are more deformable and elongate over a longer time as they cross. This phenomenon can be seen clearly in figure 15 for $\Delta x_2^0/2a = 1$.

The overall effect of capsule deformability and initial separation is summarized in figure 16 where we show the net cross-flow displacement $\delta_2 = (\Delta x_2^\infty - \Delta x_2^0)/2$ of each capsule as a function of ε, for different initial offsets Δx_2^0. We first note that the final displacement depends only weakly on capsule deformability as measured by ε. Obviously as $\Delta x_2^0/2a$ increases, the interaction between the two capsules weakens and δ_2 decreases. Asymptotically, for $\Delta x_2^0/a \gg 1$, the hydrodynamic interaction between the capsules becomes negligible and δ_2 tends to 0.

During strong encounters ($\Delta x_2^0/2a \leqslant 0.25$), a viscous film appears between the capsules as they pass each other and then capsule deformability plays a role. Indeed, the importance of viscous lubrication forces increases with the thinness and the width of this film. When ε increases, the particles elongate and the film widens. However, the positive pressure in the film eventually causes dimpling that results in thickening of the film (figure 17). Thus, two opposite effects (thickening and widening of the film) compete, and we find there exists a capillary number for which the cross-flow displacement δ_2 is maximum.

This result is qualitatively similar to that obtained by Loewenberg & Hinch (1997) for a pair of droplets. It is not possible to plot the results obtained by these authors in figure 16, because the capillary number calculated for droplets is based on surface

tension and cannot be compared with our elastic capillary number, based on a shear elastic modulus. Nevertheless, we can compare the crossflow displacements observed over a range of capillary numbers for a given initial offset. For closely spaced trajectories ($\Delta x_2^0/2a \leqslant 0.5$), the final deviation of a droplet is about 30% higher than that of a capsule whereas it is almost the same for higher offsets ($\Delta x_2^0/2a \geqslant 0.75$). ($\delta_2/a \approx 0.44, 0.46, 0.42, 0.39$ for surface-tension-based capillary numbers equal to 0, 0.1, 0.3, 0.4, respectively $\lambda = 1$ and $\Delta x_2^0/2a = 0.25$ (Loewenberg & Hinch 1997, figure 5), to be compared to the deviations reported in figure 16.) This indicates that the elastic membrane plays an important role in the near-contact behaviour of capsules.

Furthermore, we also note that the evolution of the stable zone as Δx_2^0 varies – zone (*a*) in figure 16 – confirms that for low initial offsets, the capsule stability strongly depends on capillary number.

5. Conclusion

The numerical technique based on Lagrangian tracking of a deformable elastic interface coupled to numerical interpolation of the deformed surface by means of bi-cubic B-spline functions is quite powerful. It allows us to model a dynamic interaction problem between two highly deformable particles over long times with very good precision. Fine mechanical phenomena such as a tendency towards buckling can also be detected. With this technique, we have been able to investigate the hydrodynamic interactions of two identical capsules freely suspended in simple shear flow. The deformability is controlled by both the capillary number ε and the membrane prestress level, measured by an inflation ratio α. Overall, the interaction remains weak as long as the distance between the two centres of mass is larger than a few initial capsule diameters. Owing to the particle deformability and the inner and outer viscous flows, the collision is irreversible and the capsule trajectories are shifted in the crossflow direction after they have passed each other.

The comparison with results obtained for interacting liquid drops by Loewenberg & Hinch (1997) and by Guido & Simeone (1998) allows us to estimate the effect of the elastic membrane on the capsule motion. The relative motion of a pair of capsules is only qualitatively similar to that of droplets because the liquid–liquid interface differs from a solid elastic membrane, particularly for the transmission of shear stress. We find that the net crossflow displacement is smaller for capsules than for droplets. This effect, particularly visible for closely spaced trajectories, is probably due to the fast and strong elastic relaxation of the capsule membrane.

For liquid droplets, Loewenberg & Hinch (1997) showed that the trajectory shift mainly depends on the viscosity ratio λ, rather than on the capillary number. Our results also show a weak dependence on ε and α. We did not investigate the effect of λ in the present study, but it would be interesting to do so since this parameter is expected to affect significantly the relaxation process and thus the final trajectory shift.

Another situation that should also be studied corresponds to the case where the two centres of mass G_1 and G_2 are not initially located in the same shear plane ($\Delta x_3^0 \neq 0$). The deviation in the vorticity direction may be expected to be smaller than along the velocity gradient (Loewenberg & Hinch 1997). However, to compute the self-diffusion coefficient of a dilute suspension of capsules, it is necessary to complete the present results with the analysis of three-dimensional trajectories.

Another aspect of this work concerns the evolution of the stress level in the membranes during the motion. This is an important point, since a capsule may unexpectedly burst when its membrane is subjected to large hydrodynamic loads. It

turns out that the interaction between the capsules causes extra tensions which might damage the membranes. In most cases, the peak of tension in the membranes appears as the capsules overlap. However, for closely spaced trajectories and small capillary numbers, high tensions appear in the near-contact regions during the separation phase. Furthermore, the interaction generates negative tensions in the membrane (and thus possible buckling instabilities) in two different processes. For very small capillary number and preinflation ratio, the instability develops during the collision, as the capsules start overlapping. For higher prestress levels ($\alpha \geqslant 2.5\%$ here, although this value depends on the membrane law), it appears above a maximum capillary number, as the two capsules separate and the membranes quickly evolve from a concave to a convex shape. This indicates that it would be interesting to include bending resistance in the membrane mechanical model to see how the post-buckling behaviour influences the particle interaction.

The authors gratefully acknowledge access to computer resources PILCAD (Plateforme Inter-Laboratoires de CAlcul Distribués) financed in part by ANVAR, HEUDYASIC and ROBERVAL laboratories (Université de Technologie de Compiègne).

REFERENCES

Barthès-Biesel, D. & Rallison, J. M. 1981 The time-dependent deformation of a capsule freely suspended in a linear shear flow. *J. Fluid Mech.* **113**, 251–267.

Barthès-Biesel, D., Diaz, A. & Dhenin, E. 2002 Effect of constitutive laws for two-dimensional membranes on flow-induced capsule deformation. *J. Fluid Mech.* **460**, 211–222.

Batchelor, G. K. & Green, J. T. 1972 The hydrodynamic interaction of two small freely-moving spheres in a linear flow field. *J. Fluid Mech.* **56**, 375–400.

Breyiannis, G. & Pozrikidis, C. 2001 Simple shear flow of suspensions of elastic capsules. *Theoret. Comput. Fluid Dyn.* **13**, 327–347.

Chang, K. S. & Olbricht, W. L. 1993 Experimental studies of the deformation and breakup of a synthetic capsule in steady and unsteady simple shear flow. *J. Fluid Mech.* **250**, 609–633.

Charles, R. & Pozrikidis, C. 1998 Signicance of the dispersed-phase viscosity on the simple shear flow of suspensions of two-dimensional liquid drops. *J. Fluid Mech.* **365**, 205–233.

Guido, S. & Simeone, M. 1998 Binary collision of drops in shear flow by computer-assisted video optical microscopy. *J. Fluid Mech.* **357**, 1–20.

Lac, E. & Barthès-Biesel, D. 2005 Deformation of a capsule in simple shear flow: effect of membrane prestress. *Phys. Fluids* **17**, 072105.

Lac, E., Barthès-Biesel, D., Pelekasis, N. A. & Tsamopoulos, J. 2004 Spherical capsules in three-dimensional unbounded Stokes flow: effect of the membrane constitutive law and onset of buckling. *J. Fluid Mech.* **516**, 303–334.

Loewenberg, M. & Hinch, E. J. 1997 Collision of two deformable drops in shear flow. *J. Fluid Mech.* **338**, 299–315.

Pozrikidis, C. 1992 *Boundary Integral and Singularity Methods for Linearized Viscous Flow*. Cambridge University Press.

Pozrikidis, C. 1995 Finite deformation of liquid capsules enclosed by elastic membranes in simple shear flow. *J. Fluid Mech.* **297**, 123–152.

Pozrikidis, C. 2003 *Modelling and Simulation of Capsules and Biological Cells*. Chapman & Hall/CRC.

Ramanujan, S. & Pozrikidis, C. 1998 Deformation of liquid capsules enclosed by elastic membranes in simple shear flow: large deformations and the effect of capsule viscosity. *J. Fluid Mech.* **361**, 117–143.

Sherwood, J. D., Risso, F., Collé-Paillot, F., Edwards-Lévy, F. & Lévy, M. C. 2003 Transport rates through a capsule membrane to attain Donnan equilibrium. *J. Colloid Interface Sci.* **263**, 202–212.

Skalak, R., Tozeren, A., Zarda, R. P. & Chien, S. 1973 Strain energy function of red blood cell membranes. *Biophys. J.* **13**, 245–264.

Van de Ven, T. G. & Mason, S. G. 1976 Pairs of interacting spheres in shear flow. *J. Colloid Interface Sci.* **57**, 505–516.

Walter, A., Rehage, H. & Leonhard, H. 2000 Shear-induced deformation of polyamid microcapsules. *Colloid Polymer Sci.* **278**, 169–175.

Walter, A., Rehage, H. & Leonhard, H. 2001 Shear induced deformation of microcapsules: shape oscillations and membrane folding. *Colloids and Surfaces* A: *Physicochem. Engng Aspects* **183–185**, 123–132.